Article

Structure-Guided Design of AMP Mimics That Inhibit Fructose-1,6-bisphosphatase with High Affinity and Specificity

Mark D. Erion, Qun Dang, M. Rami Reddy, Srinivas Rao Kasibhatla, Jingwei Huang, William N. Lipscomb, and Paul D. van Poelje

J. Am. Chem. Soc., **2007**, 129 (50), 15480-15490 • DOI: 10.1021/ja074869u

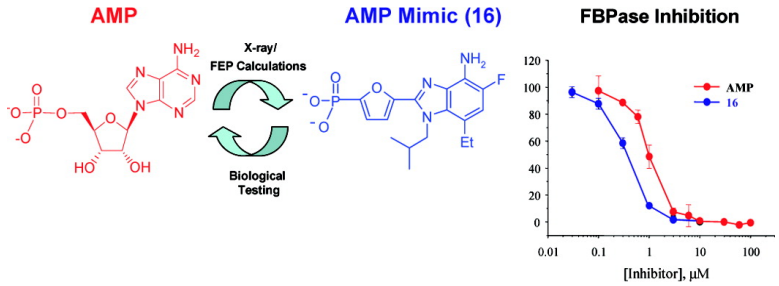

More About This Article

Additional resources and features associated with this article are available within the HTML version:

- Supporting Information
- Links to the 3 articles that cite this article, as of the time of this article download
- Access to high resolution figures
- Links to articles and content related to this article
- Copyright permission to reproduce figures and/or text from this article

View the Full Text HTML

J|A|C|S
ARTICLES
Published on Web 11/28/2007

Structure-Guided Design of AMP Mimics That Inhibit Fructose-1,6-bisphosphatase with High Affinity and Specificity

Mark D. Erion,*,† Qun Dang,† M. Rami Reddy,† Srinivas Rao Kasibhatla,†,‡ Jingwei Huang,§ William N. Lipscomb,§ and Paul D. van Poelje†

Contribution from the Departments of Medicinal Chemistry, Biochemistry, and Molecular Modeling, Metabasis Therapeutics, Inc., 11119 North Torrey Pines Road, La Jolla, California 92037, and Department of Chemistry and Chemical Biology, Harvard University, Cambridge, Massachusetts 02138

Received July 2, 2007; E-mail: erion@mbasis.com

Abstract: AMP binding sites are commonly used by nature for allosteric regulation of enzymes controlling the production and metabolism of carbohydrates and lipids. Since many of these enzymes represent potential drug targets for metabolic diseases, efforts were initiated to discover AMP mimics that bind to AMP-binding sites with high affinity and high enzyme specificity. Herein we report the structure-guided design of potent fructose 1,6-bisphosphatase (FBPase) inhibitors that interact with the AMP binding site on FBPase despite their structural dissimilarity to AMP. Molecular modeling, free-energy perturbation calculations, X-ray crystallography, and enzyme kinetic data guided our redesign of AMP, which began by replacing the 5′-phosphate with a phosphonic acid attached to C8 of the adenine base via a 3-atom spacer. Additional binding affinity was gained by replacing the ribose with an alkyl group that formed van der Waals interactions with a hydrophobic region within the AMP binding site and by replacing the purine nitrogens N1 and N3 with carbons to minimize desolvation energy expenditures. The resulting benzimidazole phosphonic acid, **16**, inhibited human FBPase ($IC_{50} = 90$ nM) 11-fold more potently than AMP and exhibited high specificity for the AMP binding site on FBPase. **16** also inhibited FBPase in primary rat hepatocytes and correspondingly resulted in concentration-dependent inhibition of the gluconeogenesis pathway. Accordingly, these results suggest that the AMP site of FBPase may represent a potential drug target for reducing the excessive glucose produced by the gluconeogenesis pathway in patients with type 2 diabetes.

Introduction

Adenosine 5′-monophosphate (AMP) and the related nucleoside adenosine are increasingly recognized as important physiological sensors of cellular energy status that modulate consumption and production of energy during times of cellular stress.[1] Both are produced from intracellular ATP stores during net ATP breakdown to minimize further decreases in ATP. Significant decreases in cellular ATP levels arising from increased ATP catabolism (e.g., during exercise) or decreased ATP production (e.g., as a consequence of oxygen deprivation or mitochondrial toxicity) lead to disruption of essential cellular processes and cell death. Adenosine preserves ATP levels through activation of extracellular adenosine receptors, which leads to decreased ATP consuming activities (e.g., neuron firing, muscle contraction) and increased ATP production through enhanced blood flow and oxygen supply.[2] In contrast, AMP acts intracellularly to preserve ATP levels through simultaneous inhibition of pathways that consume ATP (e.g., gluconeogenesis and cholesterol biosynthesis) and activation of pathways that produce ATP (e.g., glycolysis, glycogenolysis, and free fatty acid β-oxidation).[3]

AMP increases intracellular ATP levels in large part by regulating flux through pathways governing carbohydrate and lipid biosynthesis and metabolism (Figure 1). AMP acts by directly or indirectly modulating the activity of the key rate-controlling enzymes in these pathways. Catalytic activity is typically affected through the binding of AMP to allosteric sites, which may therefore represent potential drug targets for metabolic diseases such as diabetes, hyperlipidemia, and hypercholesterolemia. For example, the AMP binding enzymes, fructose-1,6-bisphosphatase[4] (FBPase) and glycogen phosphorylase[5] (GP), control the flux through the gluconeogenesis and glycogenolysis pathways, respectively, and therefore represent potential drug targets for reducing the excessive glucose

† Metabasis Therapeutics.
‡ Present address: Biogen Idec, 5200 Research Place, San Diego, CA 92122.
§ Harvard University.

(1) (a) Hardie, D. G. *Nature* **1994**, *370*, 599−600. (b) Hardie, D. G.; Hawley, S. A. *Bioessays* **2001**, *23*, 1112−1119. (c) Kahn, B. B.; Alquier, T.; Carling, D.; Hardie, D. G. *Cell Metab.* **2005**, *1*, 15−25. (d) Hardie, D. G.; Hawley, S. A.; Scott, J. W. *J. Physiol.* **2006**, *574*, 7−15.
(2) (a) Schrader, J. *Circulation* **1990**, *81*, 389−391. (b) Erion, M. D. *Annu. Rep. Med. Chem.* **1993**, *28*, 295−304.
(3) Hardie, D. G. *Rev Endocr. Metab. Disord.* **2004**, *5*, 119−125.
(4) (a) Benkovic, S. J.; deMaine, M. M. *Adv. Enzymol. Relat. Areas Mol. Biol.* **1982**, *53*, 45−82. (b) Ke, H. M.; Liang, J. Y.; Zhang, Y. P.; Lipscomb, W. N. *Biochemistry* **1991**, *30*, 4412−4420. (c) Ke, H. M.; Zhang, Y. P.; Lipscomb, W. N. *Proc. Natl. Acad. Sci. U.S.A.* **1990**, *87*, 5243−5247. (d) Shyur, L.-F.; Aleshin, A. E.; Honzatko, R. B.; Fromm, H. J. *J. Biol. Chem.* **1996**, *271*, 33301−33307.
(5) Barford, D.; Hu, S. H.; Johnson, L. N. *J. Mol. Biol.* **1991**, *218*, 233−260.

10.1021/ja074869u CCC: $37.00

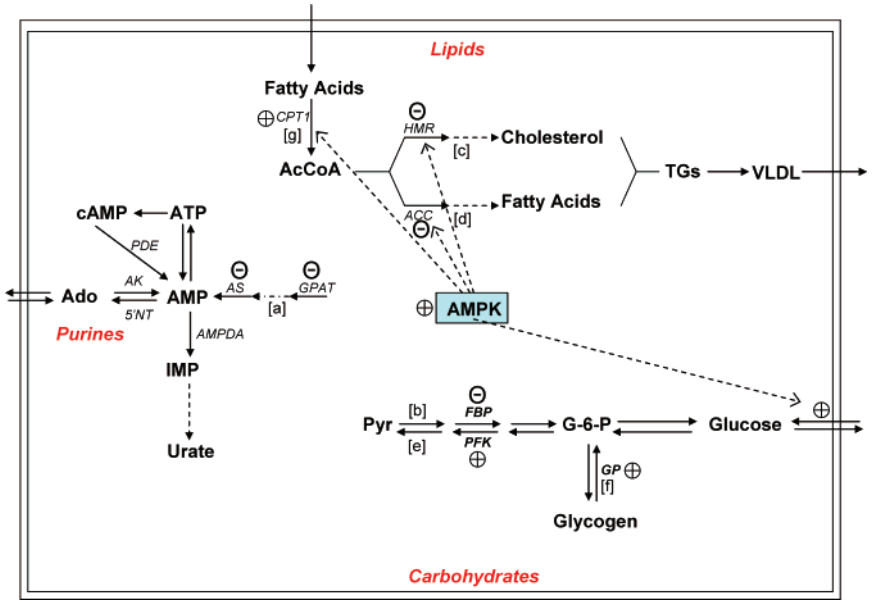

Figure 1. Pathways and enzymes that either affect intracellular AMP levels or are regulated by AMP. AMP is synthesized by either the *de novo* purine synthesis pathway [a], ATP degradation, cAMP hydrolysis, or Ado phosphorylation. AMP is metabolized either by phosphorylation to ATP, deamination to IMP, or dephosphorylation to Ado. AMP inhibits pathways that consume energy such the purine [a], glucose (gluconeogenesis) [b], cholesterol [c], and fatty acid [d] biosynthesis pathways. AMP activates pathways that produce energy such as glycolysis [e], glycogenolysis [f], and fatty acid oxidation [g]. AMP affects these pathways by inhibiting (−) or activating (+) key rate-controlling enzymes either directly through allosteric binding sites or indirectly by first activating AMP activated protein kinase (AMPK), which in turn affects the activity of the indicated enzymes through protein phosphorylation. Abbreviations: ACC, acetyl CoA carboxylase; Ado, adenosine; AK, adenosine kinase; AMPDA, AMP deaminase; AMPK, AMP-activated protein kinase; AS, adenylosuccinate synthetase; CPT1, carnitine palmitoyltransferase-1; FBP, fructose-1,6-bisphosphatase; G-6-P, glucose-6-phosphate; GPAT, glutamine phosphoribosylpyrophosphate amidotransferase; GP, glycogen phosphorylase; HMR, HMG CoA reductase; 5′NT, 5′-nucleotidase; PDE, phosphodiesterase; PFK, phosphofructokinase; Pyr, pyruvate; TGs, triglycerides; VLDL, very low-density lipoprotein.

production that accompanies type 2 diabetes.[6] Another AMP-binding enzyme generating considerable interest as a potential drug target is AMP-activated protein kinase[7] (AMPK), which affects cholesterol, fatty acid, and triglyceride biosynthesis as well as fatty acid oxidation by phosphorylating the rate-limiting enzymes in these pathways (e.g., HMG CoA reductase and acetyl-CoA carboxylase).

Despite numerous discovery programs over the past 20 years targeting various AMP-binding enzymes, few compounds have emerged with suitable potency, specificity, and biological activity. Screening large, diverse compound libraries for AMP deaminase (AMPDA) inhibitors, FBPase inhibitors,[8] GP inhibitors,[9] and more recently AMPK activators[10] failed to identify compounds with high affinity for the AMP site. Failure was attributed to the local environment within these sites, which unlike most drug binding sites is hydrophilic and highly dependent on hydrogen bond interactions. Since hydrogen bond strength is sensitive to both distance and bond angle, compounds with the desired affinity not only had to possess the complementary hydrogen bond donor and acceptor groups but also had to have a structure that properly aligned each within the binding site. These strict structural requirements were met most readily by close structural analogs of AMP, which as a compound class proved to be unsuitable as AMP mimics because of their inability to achieve the desired cellular activity due to poor plasma stability and cell penetration properties. Efforts to find nucleoside analogs that generate nucleoside monophosphates (NMPs) inside cells capable of functioning as potent and specific AMP mimics were also unsuccessful. Failure stemmed from the inability of most nucleoside analogs to generate high intracellular levels of the NMP either because of poor initial phosphorylation[11] or because the NMP was rapidly phosphorylated to the corresponding nucleoside triphosphate. 5-Aminoimidazole-4-carboxamide 1-β-D-ribofuranoside (AICA riboside), a nucleoside analog we serendipitously discovered in the late 1980s to lower glucose levels,[12] was one of the rare exceptions. Unfortunately, the monophosphate (ZMP, Chart 1) that accumulated inside hepatocytes proved to be a relatively poor AMP mimic that interacted nonspecifically with numerous AMP-binding enzymes, including FBPase,[13] GP,[14] AMPK,[15] and phosphofructokinase (PFK).[16]

(6) (a) DeFronzo, R. A. *Diabetes* **1988**, *37*, 667−687. (b) Magnusson, I.; Rothman, D. L.; Katz, L. D.; Shulman, R. G.; Shulman, G. I. *J. Clin. Invest.* **1992**, *90*, 1323−1327. (c) Pilkis, S. J.; Granner, D. K. *Annu. Rev. Physiol.* **1992**, *54*, 885−909.
(7) Hardie, D. G. *Annu. Rev. Pharmacol. Toxicol.* **2007**, *47*, 185−210.
(8) (a) Choe, J. Y.; Nelson, S. W.; Arienti, K. L.; Axe, F. U.; Collins, T. L.; Jones, T. K.; Kimmich, R. D.; Newman, M. J.; Norvell, K.; Ripka, W. C.; Romano, S. J.; Short, K. M.; Slee, D. H.; Fromm, H. J.; Honzatko, R. B. *J. Biol. Chem.* **2003**, *278*, 51176−51183. (b) Wright, S. W.; et al. *J. Med. Chem.* **2002**, *45*, 3865−3877. (c) Wright, S. W.; Carlo, A. A.; Danley, D. E.; Hageman, D. L.; Karam, G. A.; Mansour, M. N.; McClure, L. D.; Pandit, J.; Schulte, G. K.; Treadway, J. L.; Wang, I. K.; Bauer, P. H. *Bioorg. Med. Chem. Lett.* **2003**, *13*, 2055−2058. (d) Wright, S. W.; Hageman, D. L.; McClure, L. D.; Carlo, A. A.; Treadway, J. L.; Mathiowetz, A. M.; Withka, J. M.; Bauer, P. H. *Bioorg. Med. Chem. Lett.* **2001**, *11*, 17−21. (e) Lai, C.; Gum, R. J.; Daly, M.; Fry, E. H.; Hutchins, C.; Abad-Zapatero, C.; von Geldern, T. W. *Bioorg. Med. Chem. Lett.* **2006**, *16*, 1807−1810. (f) von Geldern, T. W.; Lai, C.; Gum, R. J.; Daly, M.; Sun, C.; Fry, E. H.; Abad-Zapatero, C. *Bioorg. Med. Chem. Lett.* **2006**, *16*, 1811−1815.
(9) (a) Kristiansen, M.; Andersen, B.; Iversen, L. F.; Westergaard, N. *J. Med. Chem.* **2004**, *47*, 3537−3545. (b) Hoover, D. J.; Lefkowitz-Snow, S.; Burgess-Henry, J. L.; Martin, W. H.; Armento, S. J.; Stock, I. A.; McPherson, R. K.; Genereux, P. E.; Gibbs, E. M.; Treadway, J. L. *J. Med. Chem.* **1998**, *41*, 2934−2938.
(10) Cool, B.; Zinker, B.; Chiou, W.; Kifle, L.; Cao, N.; Perham, M.; Dickinson, R.; Adler, A.; Gagne, G.; Iyengar, R.; Zhao, G.; Marsh, K.; Kym, P.; Jung, P.; Camp, H. S.; Frevert, E. *Cell Metab.* **2006**, *3*, 403−416.
(11) Yamanaka, G.; Wilson, T.; Innaimo, S.; Bisacchi, G. S.; Egli, P.; Rinehart, J. K.; Zahler, R.; Colonno, R. J. *Antimicrob. Agents Chemother.* **1999**, *43*, 190−193.
(12) Gruber, H. E. US Patent 5,658,889, August 19, 1997.

Chart 1

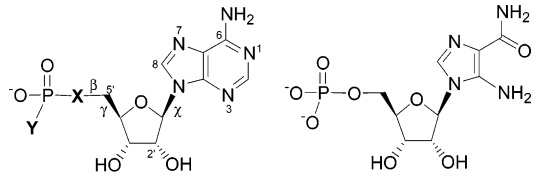

AMP	X = O	Y = O^-
1	X = CH_2	Y = O^-
2	X = O	Y = CH_3

ZMP

With little hope that NMPs could be found with sufficient potency and specificity to serve as drug candidates, we turned our attention to non-nucleoside AMP mimics and used a structure-based drug design strategy to help guide our discovery efforts. Reported herein is the design and discovery of the lead FBPase inhibitor series that demonstrates the potential of AMP binding sites as drug targets. Following this manuscript is an article[17] that describes our lead optimization efforts that led to the discovery of MB05032 and the MB05032 prodrug MB06322 (CS-917): a compound that significantly reduces glucose levels in animal models of type 2 diabetes[18,19] as well as in diabetic patients.[20]

Results

Design Strategy. AMP binds to FBPase at an allosteric binding site and either induces a protein conformational change from the R-state (high catalytic activity) to the T-state (low catalytic activity) or acts to stabilize the T-state.[4] Thus, the challenge we faced at the outset of our program was to find an AMP mimic that not only bound to FBPase with high affinity but also favored the R- to T-protein conformational change. In addition, results from earlier efforts evaluating AMP analog specificity suggested that complete discrimination between the AMP binding site of FBPase and those of other AMP-binding enzymes would likely require the AMP mimic to be as structurally dissimilar to AMP as possible. Last, the AMP mimic also needed to be both metabolically stable and cell penetrable to reach intracellular levels required for effective inhibition of FBPase and the gluconeogenesis pathway. With these general criteria in mind, our design efforts began by focusing on the 5′-phosphate and its interactions with the AMP binding site. Inhibition studies showed that removal of the phosphate resulted in a $>10^6$-fold decrease in inhibitory potency (data not shown). X-ray structures of porcine FBPase complexed with AMP[5b,c] (1FBP) and human FBPase complexed with AMP[21] (1FTA) and ZMP[22] suggested that the decrease in potency was likely due to the loss of seven hydrogen bonds formed between the phosphate and residues in the positively charged phosphate binding site (Figure 2). Accordingly, our first design challenge was to identify a phosphate surrogate that retained most of the associated binding affinity but, unlike organophosphates, exhibited good stability in biological fluids.

Given the location and orientation of the hydrogen bond donors within the phosphate binding site, most of the design strategies incorporated tetrahedral, negatively charged phosphate surrogates rather than non-tetrahedral groups such as carboxylic acids.[23] The phosphonic acid group was particularly attractive as a phosphate surrogate, since it represents a close structural analog and is resistant to phosphatases. Somewhat surprisingly, simple phosphonate analogs of AMP (**1**−**2**, Chart 1) exhibited a >2000-fold decrease in inhibitory potency (data not shown). Free-energy calculations and inhibition studies using the Y113F mutant[21a] suggested that the loss in inhibitor potency for **1** was at least partially due to the loss in the hydrogen bond between Y113 and the 5′ oxygen.[24] Decomposing the relative binding free-energy difference into van der Waals and electrostatic energies showed that most of the lost affinity was due to decreases in electrostatic energy, which was attributed primarily to less favorable interaction energies with Y113, K112, and L30.[24d]

These results prompted a further examination of the FBPase-AMP complex, which led to the realization that the phosphate binding site might be accessible from the purine base. The binding conformation of AMP and associated torsion angles [χ (glycosidic bond, $C_4-N_9-C_{1'}-O_{1'}$) = −153°; γ ($O_{5'}-C_{5'}-C_{4'}-C_{3'}$) = 64°; β ($P-O_{5'}-C_{5'}-C_{4'}$) = −140°] orient the adenine base such that the C8−H bond points directly toward the phosphate binding site (Figure 2). Accordingly, our initial goal was to identify molecular fragments that could link the purine base with a phosphonic acid in a manner that preserved the key interactions within both the purine and phosphate binding sites.

Spacer Optimization. Using a computer model developed from the X-ray structure of the human liver FBPase−ZMP complex,[22a] molecular fragments (termed spacer groups) of 1−5 atoms in length were attached to C8 and the phosphorus atom, with the ribose either removed or allowed to freely move. Low energy conformations were energy minimized in solvent after

(13) (a) Vincent, M. F.; Marangos, P. J.; Gruber, H. E.; Van den Berghe, G. *Diabetes* **1991**, *40*, 1259−1266. (b) Vincent, M. F.; Erion, M. D.; Gruber, H. E.; Van den Berghe, G. *Diabetologia* **1996**, *39*, 1148−1155.

(14) Longnus, S. L.; Wambolt, R. B.; Parsons, H. L.; Brownsey, R. W.; Allard, M. F. *Am. J. Physiol. Regul. Integr. Comp. Physiol.* **2003**, *284*, R936−R944.

(15) van den Berghe, G. *PCT Appl.* US92/06828. (b) Sullivan, J. E.; Brocklehurst, K. J.; Marley, A. E.; Carey, F.; Carling, D.; Beri, R. K. *FEBS Lett.* **1994**, *353*, 33−36. (c) Merrill, G. F.; Kurth, E. J.; Hardie, D. G.; Winder, W. W. *Am. J. Physiol.* **1997**, *273*, E1107−E1112.

(16) Vincent, M. F.; Bontemps, F.; Van den Berghe, G. *Biochem. J.* **1992**, *281*, 267−272.

(17) Dang, Q.; Kasibhatla, S. R.; Reddy, M. R.; Jiang, T.; Reddy, K. R.; van Poelje, P. D.; Huang, J.; Lipscomb, W. N.; Erion, M. D. *J. Am. Chem. Soc.* **2007**, *129*, 15491−15502.

(18) Erion, M. D.; van Poelje, P. D.; Dang, Q.; Kasibhatla, S. R.; Potter, S. C.; Reddy, M. R.; Reddy, K. R.; Jiang, T.; Lipscomb, W. N. *Proc. Natl. Acad. Sci. U.S.A.* **2005**, *102*, 7970−7975.

(19) van Poelje, P. D.; Potter, S. C.; Chandramouli, V. C.; Landau, B. R.; Dang, Q.; Erion, M. D. *Diabetes* **2006**, *55*, 1747−1754.

(20) Triscari, J.; Walker, J.; Feins, K.; Tao, B.; Bruce, S. R. *Diabetes* **2006**, *55* (Suppl 1), 444P.

(21) (a) Gidh-Jain, M.; Zhang, Y.; van Poelje, P. D.; Liang, J. Y.; Huang, S.; Kim, J.; Elliott, J. T.; Erion, M. D.; Pilkis, S. J.; Raafat el-Maghrabi, M.; Lipscomb, W. N. *J. Biol. Chem.* **1994**, *269*, 27732−27738. (b) Iversen, L. F.; Brzozowski, M.; Hastrup, S.; Hubbard, R.; Kastrup, J. S.; Larsen, I. K.; Naerum, L.; Norskov-Lauridsen, L.; Rasmussen, P. B.; Thim, L.; Wiberg, F. C.; Lundgren, K. *Protein Sci.* **1997**, *6*, 971−982.

(22) (a) Lipscomb, W. N. Unpublished results. The ZMP binding conformation is closely related to the AMP binding conformation found in the human FBPase (ref 21a) and pig kidney FBPase (1FBP, ref 4b) structures. (b) ref 21b.

(23) Carboxylic acids were used previously in the design of a series of AMP deaminase inhibitors. High affinity was achieved despite suboptimal interactions in the phosphate binding site by using transition-state mimicry. Erion, M. D.; Srinivas, R. K.; Bookser, B. C.; van Poelje, P. D.; Reddy, M. R.; Gruber, H. E.; Appleman, J. R. *J. Am. Chem. Soc.* **1999**, *121*, 308−319.

(24) (a) Erion, M. D.; van Poelje, P. D.; Reddy, M. R. *J. Am. Chem. Soc.* **2000**, *122*, 6114−6115. (b) Reddy, M. R.; Erion, M. D. *J. Am. Chem. Soc.* **2001**, *123*, 6246−6252. (c) Reddy, M. R.; Erion, M. D. In *Free Energy Calculations in Rational Drug Design*; Reddy, M. R., Erion, M. D., Eds.; Kluwer/Plenum Press: New York, 2001; pp 285−297. (d) Reddy, M. R.; Erion, M. D. *J. Am. Chem. Soc.* **2007**, *129*, 9296−9297.

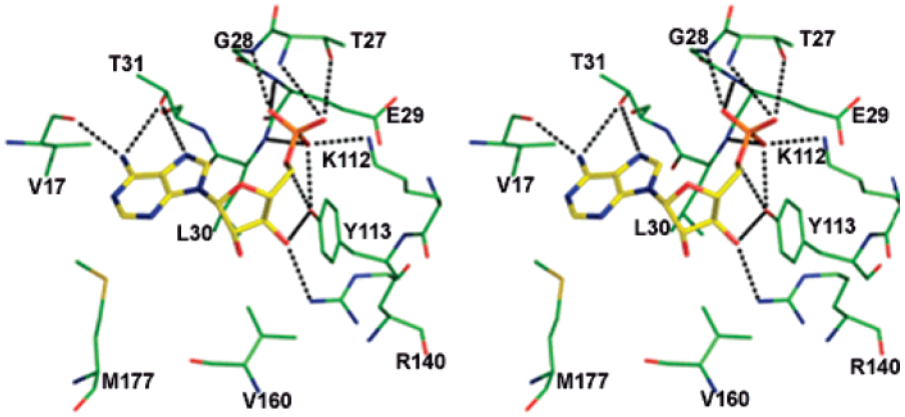

Figure 2. Stereodiagram of the AMP binding conformation and binding site interactions present in the computer model of the human FBPase−AMP complex that was generated from the X-ray structure of the FBPase−ZMP complex (see Methods). Dashed lines designate hydrogen bond interactions between AMP and the denoted FBPase binding site residues.

Table 1. Interaction Energies of 8-Substituted Adenosine Analogs

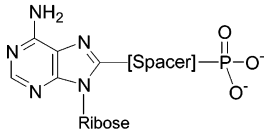

spacer (C8 → P)	C8–P[a,b] (Å)	H_2N–P[a,c] (Å)	IE[d] (kcal/mol)
$N(H)CH_2$	4.08	6.20	11.8
$N(H)CH_2CH_2$	5.16	6.96	−35.7
$N(H)CH_2CH_2CH_2$	6.14	8.02	33.5
$CH_2N(H)CH_2$	5.20	6.98	−9.9
CH_2CH_2	4.24	6.42	3.4
$CH_2CH_2CH_2$	5.31	7.09	−43.6
$CH_2CH_2CH_2CH_2$	6.30	8.16	28.8
CH_2OCH_2	4.91	7.05	−38.9
2,5-furanyl	5.18	7.75	−69.2
$C(=O)CH_2$	5.10	6.96	10.5
$C(=N)HCH_2$	4.98	6.85	−2.7
$CH=CHCH_2$ (cis)	5.05	6.88	−5.6
$CH=CHCH_2$ (trans)	5.17	7.01	−19.7

[a] Through space distance between designated atoms in energy minimized structure. [b] Distance is 4.24 Å for AMP complexed to human FBPase. [c] Distance is 7.27 Å for AMP complexed to human FBPase. [d] Interaction energy determined as described in Methods section.

Table 2. Structure Activity Relationships

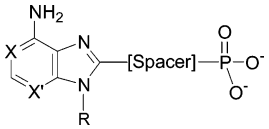

cmpd	spacer	X	X′	R	IC_{50} (μM)
AMP					1 ± 0.05
ZMP					12 ± 1.4
3	$N(H)CH_2$	N	N	ribose	>1000[a]
4	$N(H)CH_2CH_2$	N	N	ribose	118 ± 9
5	$N(H)(CH_2)_3$	N	N	ribose	>1000[b]
6	$N(H)CH_2CH_2$	N	N	H	500 ± 10
7	$N(H)CH_2$	N	N	*c*hexylethyl	∼1000
8	$N(H)CH_2CH_2$	N	N	*c*hexylethyl	97 ± 20
9	$CH_2CH_2CH_2$	N	N	*c*hexylethyl	26 ± 1
10	CH_2OCH_2	N	N	*c*hexylethyl	15 ± 3
11	2,5-furanyl	N	N	phenethyl	5 ± 0
12	2,5-furanyl	N	N	*c*hexylethyl	1.2 ± 0.9
13	2,5-furanyl	N	N	*i*Bu	2.2 ± 0.2
14	2,5-furanyl	N	N	*neo*Pentyl	1.1 ± 0.2
15	2,5-furanyl	CH	CH	*i*Bu	1.6 ± 0.1
16	2,5-furanyl	CF	C−Et	*i*Bu	0.09 ± 0.1

[a] Inhibition is 27% at 1 mM. [b] Inhibition is 33% at 1 mM

docking in the AMP binding site using a four-stage protocol. The minimized structures were then used in calculations of interaction energies and ligand strain energies (Table 1). The energy minimized complexes were also evaluated graphically for the ability of these low-energy spacer conformations to replicate the hydrogen bond networks formed by AMP within the phosphate and purine binding sites. The results, while qualitative, suggested that the molecular fragments that most optimally bridged the space between C8 and P contained 3 contiguous atoms and a length of 4.9−5.3 Å (Table 1).

Synthesis and analysis of the inhibition kinetics of 8-aminoadenosine analogs with an alkyl phosphonic acid attached to the 8-amino group (2- to 4-atom spacers) provided the first experimental data supporting the concept and the preference for a 3-atom spacer (Table 2, compounds **3**−**5**). Subsequent analogs confirmed these findings (Table 2, compounds **7**−**8**) and led to efforts to improve the inhibition potency, which was at least 15-fold weaker than AMP but still more potent than phosphonate **1**. Analogs covering over 22 different spacers were synthesized and evaluated (unpublished data). A modest increase in potency (∼2-fold) was achieved by replacing the all carbon spacer with an ether spacer (e.g., **9** vs **10**). Subsequent efforts focused on restricting the conformational freedom[25] of the ether led to the discovery of the 2,5-furanyl spacer (e.g., **12**), which provided an additional ∼10-fold increase in inhibitory potency.

Ribose Replacement. Linking the phosphonate to the adenine through C8 eliminated the need for the ribose as the link. Analysis of the X-ray structures of FBPase−AMP complexes placed the ribosyl moiety of AMP near the solvent interface and in position to form 2 hydrogen bonds (O5′ and O3′) with the protein. Free-energy perturbation (FEP) calculations showed that the hydrogen bonds between the 3′ hydroxyl and R140/Y113 contributed little to the overall binding affinity.[24] A Connolly surface map[26] color coded by atomic polarity showed that a portion of the volume accessible to substituents attached to N9 is relatively hydrophilic and exposed to solvent (Figure 3). In addition, the map revealed a hydrophobic surface located along the edge of the adenine base between N9 and N3/C2 composed of side chain atoms from three residues, namely

(25) Chang, C. A.; Chen, W.; Gilson, M. K. *Proc. Natl. Acad. Sci. U.S.A.* **2007**, *104*, 1534−1539.
(26) Connolly, M. L. *Science* **1983**, *221*, 709−713.

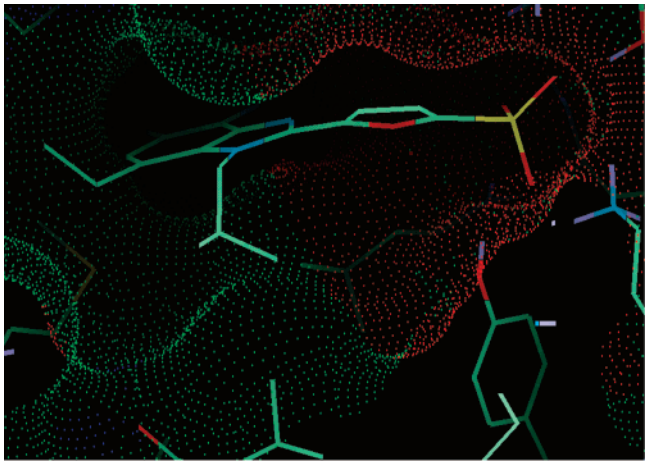

Figure 3. Connolly surface generated using the structure of the human FBPase−ZMP complex. ZMP was replaced with **16** in the binding conformation present in the FBPase−**16** model. The surface was generated using a van der Waals radius of 1.4 Å. The surface is color coded based on electrostatic potential with surface points colored red indicating positive charge, green indicating neutral, and blue indicating negative charge.

Scheme 1. Preparation of **14**[a]

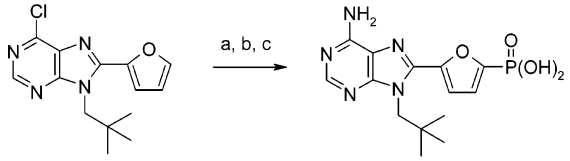

[a] Reagents and conditions: (a) LDA, THF, −78 °C; $ClP(O)(OEt)_2$, 90%; (b) ammonia, DMSO−THF, 25 °C, 56%; (c) TMSBr, CH_2Cl_2, 97%.

M177, L30, and V160. Consistent with our predictions derived from these structural findings, removal of the ribose led to less than a 5-fold loss in potency (compound **6** vs **4**, Table 2), whereas replacement of the ribose with a cyclohexylethyl group afforded comparable potency (compound **8** vs **4**). As noted above, incorporation of the 2,5-furanyl spacer in this series provides a major boost in potency (compound **12** vs **8**), independent of the alkyl group (compounds **11**, **13**, and **14**).

Purine Base Optimization. FEP calculations and experimental data suggested that the hydrogen bonds identified in the X-ray structure of the FBPase−AMP complex between FBPase and both the N7 and the $^6NH_2$ groups contribute significantly to the overall binding affinity.[24] In contrast, neither N1 nor N3 formed a favorable interaction, and both were associated with significant desolvation costs (0.7 and 1.1 kcal/mol, respectively) that could be avoided by replacement with CH.[24] Synthesis of the corresponding benzimidazole analog (**15**) showed no loss in inhibitory potency but little benefit. Fortunately, synthesis of benzimidazole analogs with various substituents attached to these carbons led to further gains in inhibitory potency and to the lead compound **16**, a compound with 24-fold greater potency than the corresponding purine analog **13** and a potency 11-fold greater than AMP (Table 2).

Synthesis of Lead Compounds. The purine **14** was efficiently synthesized from 6-chloro-8-(2-furanyl)-9-neopentylpurine (**17**) (Scheme 1), which was prepared as previously described.[27] Lithiation of **17** with LDA followed by addition of diethyl chlorophosphate gave the corresponding diethyl phosphonate ester in 90% yield. Conversion of the 6-chloro group to the corresponding amine followed by ester hydrolysis with TMSBr gave **14** in 54% overall yield. The benzimidazole **16** was prepared from 6-bromo-4-fluoro-3-nitro-1,2-benzenediamine (**18**) (Scheme 2), which was synthesized via a 2,1,3-benzoselenadiazole intermediate according to a reported procedure with some modifications.[28] Selective reductive amination of the more reactive 1-amino group with isobutyraldehyde in near quantitative yield followed by an iron (III) chloride-promoted cyclization reaction with 5-diethylphosphono-2-furaldehyde gave the benzimidazole **19** in 52% yield. The ethyl group was introduced via a Stille coupling with tributylvinyl tin followed by hydrogenation. Hydrolysis of the diethyl ester with TMSBr gave **16** in 78% overall yield from bromide **19**.

Scheme 2 [a]

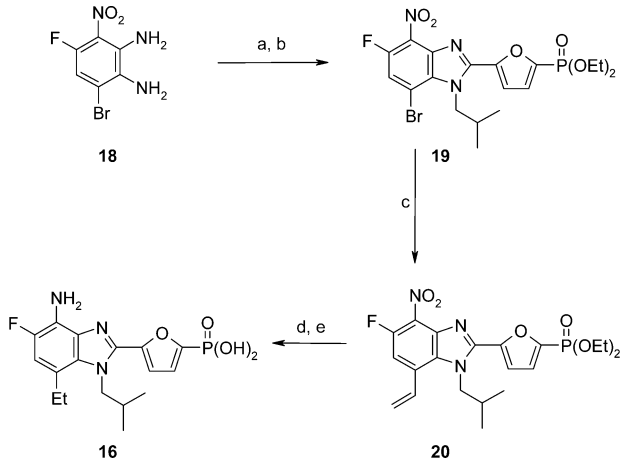

[a] Conditions: (a) *i*Pr-CHO, $NaBH(OAc)_3$, $ClCH_2CH_2Cl$, 98%; (b) $FeCl_3$, 5-diethylphosphono-2-furaldehyde, DMF, 90 °C, 52%; (c) vinyl-$SnBu_3$, $Pd(PPh_3)_2Cl_2$, DMF, 92%; (d) H_2, Pd−C, EtOH, 99%; (e) TMSBr, CH_2Cl_2, 86%.

Free-Energy Calculations. A series of *post hoc* FEP calculations[29] provided insight into the molecular interactions contributing to the inhibitory potencies of the lead compounds (Table 3). Calculations comparing close structural analogs were performed using a single topology and a total of 479 ps of molecular dynamics (MD) simulation, whereas calculations comparing analogs with more substantial structural changes were performed using the thread method and a total of 632 ps of MD simulation (see Methods). The results from the FEP calculations were consistent with the experimental findings and indicated that two-atom and four-atom spacers were associated with reduced binding affinities relative to the three-atom spacers, which typically bridged the space between C8 and P without making unfavorable contacts and with retention of nearly the full set of hydrogen bonds formed between AMP and the purine and phosphate binding sites. In the modeled structure of FBPase−**16**, the phosphonate forms six hydrogen bonds, including a hydrogen bond with Y113. The furanyl spacer is tilted slightly out of plane relative to the benzimidazole with its oxygen atom, forming a weak electrostatic contact with the NH of L30 (4.5 Å). The amino group retains the two hydrogen

(27) Dang, Q.; Brown, B. S.; Erion, M. D. *Tetrahedron Lett.* **2000**, *41*, 6559−6562.

(28) Pesin, V. G.; D'yachenko, S. A.; Khaletskii, A. M. *J. Gen. Chem., USSR (Eng. Transt.)*, **1964**, *34*, 3807−3812.

(29) (a) Zwanzig, R. J. *J. Chem. Phys.* **1954**, *22*, 1420−1426. (b) Tembe, B. L.; McCammon, J. A. *Comput. Chem.* **1984**, *8*, 281−283. (c) Pearlman, D. A. In *Free Energy Calculations in Rational Drug Design*; Reddy, M. R., Erion, M. D., Eds.; Kluwer/Plenum Press: New York, 2001; pp 9−35.

Table 3. Relative Free Energies for AMP Mimics

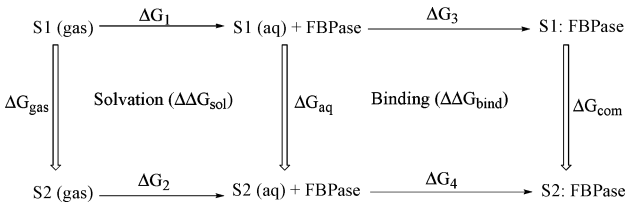

transformation (S1 → S2)		relative free energies (kcal/mol) $\Delta\Delta G_{sol}$	$\Delta\Delta G_{bind}$	$\Delta\Delta G_{bind}$ (exp)
AMP → ZMP[a,d,f]	Adenine → AICAR[b]	−1.5 ± 0.7	1.7 ± 0.9	1.6
AMP → **1**[c,e,f]	O → CH_2[c]	1.1 ± 0.5	4.6 ± 0.6	5.5
4 → **6**[d,g]	Ribose → H	3.1 ± 0.8	1.2 ± 0.9	0.8
6 → **8**[d,g]	H → *cyclo*-hexylethyl	1.3 ± 0.8	−1.7 ± 0.9	−1.4
3 → **5**[d,g]	$N(H)CH_2$ → $N(H)CH_2CH_2CH_2$	1.6 ± 0.7	−0.5 ± 0.8	−0.2
3 → **4**[d,g]	$N(H)CH_2$ → $N(H)CH_2CH_2$	1.1 ± 0.6	−1.8 ± 0.7	< −1.5
7 → **9**[e,h]	$N(H)CH_2$ → $CH_2CH_2CH_2$	2.3 ± 0.6	−2.8 ± 0.7	−2.2
8 → **9**[e,h]	$N(H)CH_2CH_2$ → $CH_2CH_2CH_2$	1.9 ± 0.6	−1.1 ± 0.7	−0.8
9 → **10**[e,h]	$CH_2CH_2CH_2$ → CH_2OCH_2	−1.5 ± 0.5	−0.8 ± 0.6	−0.4
10 → **12**[d,h]	CH_2OCH_2 → 2,5-furanyl	−0.7 ± 0.7	−2.0 ± 0.8	−1.5
13 → **15**[e,h]	X,X' = N → CH	1.4 ± 0.5	−0.6 ± 0.6	−0.2
15 → **16**[e,h]	X = CH → C−F; X' = CH → C−Et	0.9 ± 0.6	−2.2 ± 0.7	−1.9

[a] Calculation reported in ref 24c. [b] AICAR = 5-aminoimidazole-4-carboxamide 1-β-D-ribofuranoside. [c] Calculation reported in ref 24b. [d] Double topology. [e] Single topology. [f] Model generated from FBPase−ZMP X-ray structure. [g] Model generated from FBPase−**4** X-ray structure. [h] Model generated from FBPase−**11** X-ray structure.

bonds formed between the $^6NH_2$ group of AMP and residues V17 and T31 (Figure 2). Unlike AMP, however, the imidazole nitrogen of **16** forms only an electrostatic interaction with T31 and not a hydrogen bond, largely because the benzimidazole undergoes a slight in-plane rotation relative to the purine base (see X-ray crystallography results).

Relative improvements in inhibitory potency corresponding to the spacer were analyzed using FEP calculations (Table 3). Transformation of **8** to **9** ($-NHCH_2CH_2- \rightarrow -CH_2CH_2CH_2-$) and **10** to **9** ($-CH_2OCH_2- \rightarrow -CH_2CH_2CH_2-$) were associated with a 1.9 and 1.5 kcal/mol reduction in desolvation costs ($\Delta\Delta G_{sol} = \Delta G_{aq} - \Delta G_{gas}$), respectively. The unfavorable relative binding free energy associated with the latter transformation reflects a decrease in enthalpic energy arising from the loss of the electrostatic interaction with the NH of L30. Transformation of ether **10** to the 2,5-furanyl analog **12** showed that the furanyl analog is associated with a greater desolvation penalty but an overall more favorable relative free energy of binding ($\Delta\Delta G_{bind} = \Delta G_{com} - \Delta G_{aq}$ of −2.0 kcal/mol). A decrease in the entropic penalty arising from decreased conformational freedom presumably accounts for a portion of the improved binding affinity. The remaining portion is enthalpic and likely represents stronger interactions within the phosphate and purine binding sites due to the difference in the C8 to P distance (Table 1).

FEP calculations were also used to assess purine base modifications, including the effect of various substituents. Previous calculations showed that neither N1 nor N3 contributed significantly to the overall binding affinity of AMP and that both nitrogens were associated with modest desolvation penalties.[24] Consistent with these findings and the experimental results (Table 2), the relative binding free-energy difference between the purine analog **13** and benzimidazole analog **15** is −0.6 kcal/mol. FEP calculations also accurately reflected the favorable binding interactions gained by replacing the ribose with cyclohexylethyl (**4** → **6** → **8**). These transformations entailed relatively large structural perturbations and therefore required the use of the thread method[30] and long MD simulation times (632 ps). As shown in Table 3, the ribose moiety is associated with significant desolvation costs that are neutralized by a few relatively weak interactions with binding site residues. In contrast, the cyclohexylethyl is readily desolvated while making enthalpic gains through van der Waals interactions with the side chain atoms of several hydrophobic residues. Overall, the results were consistent with the inhibition potencies reported in Table 2 and the design strategy focused on enhancing inhibitory potency through replacement of the ribose with hydrophobic groups.

X-ray Structure of FBPase−Inhibitor Complexes. The three-dimensional structure of the human FBPase−**4** complex was solved to 2.8 Å resolution (W. N. Lipscomb and Y. Zhang, unpublished data) during the lead optimization phase of the discovery program. The structure confirmed the computer modeling predictions that a 3-atom spacer enabled retention of the key phosphate and purine binding site interactions. The structure also revealed that the ribosyl group was rotated away from the site it occupies in the AMP complex and toward the solvent interface. This change in glycosidic bond torsion is attributed to the relative absence of strong binding site interactions with the ribose coupled with the preference of C8-substituted purine nucleosides to exist in the *syn*-conformation.[31] More recently and years after the discovery of **16**, the structure of the FBPase−**16** complex was solved to 2.0 Å resolution (Table 4, Figure 4). Importantly, the binding site interactions determined by X-ray crystallography (Figure 5) were identical to those predicted years in advance by computer modeling (Table 5). Moreover, a comparison of the X-ray structure and the computer model showed that the binding site interaction

(30) (a) Singh, U. C.; Benkovic, S. J. *Proc. Natl. Acad. Sci. U.S.A.* **1988**, *85*, 9519−9523. (b) Reddy, M. R.; Viswanadhan, V. N.; Weinstein, J. N. *Proc. Natl. Acad. Sci. U.S.A.* **1991**, *88*, 10287−10291. (c) Reddy, M. R.; Bacquet, R. J.; Zichi, D.; Mathews, D. A.; Welsh, K. M.; Jones, T. R.; Freer, S. *J. Am. Chem. Soc.* **1992**, *114*, 10117−10122.

(31) Saenger, W. In *Principles of Nucleic Acid Structure*; Cantor, C. R., Ed.; Springer-Verlag: New York, 1984; pp 51−104.

Table 4. Data Processing and Refinement Statistics[a]

	FBPase–**16**
space group	$P2_1$
cell dimensions	$a = 67.8$ Å; $b = 83.9$ Å; $c = 280.7$ Å; $\beta = 89.9$
data collection and processing	
wavelength (Å)	0.9124
resolution (Å)	2.0 (2.07−2.00)
reflections	492 209 (16 358)
unique reflections	200 729
completeness (%)	92.0 (75.3)
multiplicity	2.5 (2.0)
R_{sym}[b] (%)	10.4 (48.3)
mean I/σ	10.1 (2.0)
number of molecules in asymmetric unit	8
refinement statistics	
$R_{working}$[c]	21.3 (32.5)
R_{free}[d]	21.9 (31.3)
average B-factor (Å^2)	22.6
R.M.S. bond (Å)	0.0061
R.M.S. angle (deg)	1.32
number of protein atoms	19 480
number of water molecules	1407

[a] Values in the parentheses apply to the outer resolution shell. [b] $R_{sym} = \sum_{hkl} \sum_i |I_i(hkl) - \langle I(hkl)\rangle| / \sum_{hkl} \sum_i I_i(hkl)$, where $I_i(hkl)$ is the intensity of an individual reflection, and $\langle I(hkl)\rangle$ is the mean intensity obtained from the multiple observations of symmetry-related reflections taken from one crystal. [c] $R_{working} = \sum_{hkl} (|F_o(hkl) - F_c(hkl)|) / \sum_{hkl}(|F_o(hkl)|)$, calculated from reflections in the working set. [d] $R_{free} = \sum_{hkl} (|F_o(hkl) - F_c(hkl)|) / \sum_{hkl}(|F_o(hkl)|)$, calculated from reflections in the test set, which is a random 5% data set selected from the whole data set.

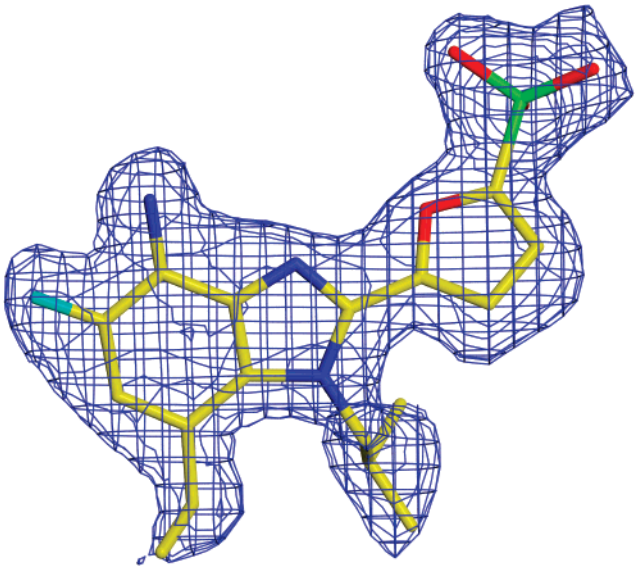

Figure 4. The $2F_o-F_c$ electron density map is contoured at 1 σ and superimposed on the refined model of the human FBPase−**16** complex at 2.0 Å resolution.

distances and binding conformation of **16** were similar (Table 5). A least-squares superposition of the Cα traces revealed only minor differences in the backbone and binding site side chain atoms (0.48 Å and 0.93 Å average rms deviations, respectively).

Superimposition of the Cα carbons of the FBPase−**16** complex onto the FBPase−AMP complex revealed only minor differences in backbone atoms and binding site side chain atoms (0.55 and 1.02 Å average rms deviations, respectively) (Figure 6). A comparison of the structures showed that **16** forms the same interactions with the phosphate and purine binding site residues as AMP with the exception of the T31 hydrogen bond

Table 5. Binding Site Interaction Distances

hydrogen bond		FBPase–**16**		FBPase–**AMP**	
ligand	residue	model[a]	X-ray[b]	model[c]	X-ray[d]
NH_2	O═C (V17)	2.61	3.33	2.76	2.98
NH_2	HO (T31)	3.16	3.19	3.07	3.23
N	HO (T31)	4.11	4.88	3.33	3.54
O (furanyl)	HN (L30)	4.32	4.56	NA	NA
$5'$O (ribose)	HO (Y113)	NA	NA	2.94	2.98
$3'$O (ribose)	HO (Y113)	NA	NA	2.94	2.53
$3'$O (ribose)	HNξ (R140)	NA	NA	2.90	2.95
OP	HN (E29)	2.54	2.70	3.10	2.78
OP	HN (G28)	2.52	3.17	2.80	2.89
OP	HO (T27)	2.87	2.58	2.92	2.73
OP	HN (T27)	3.19	2.76	3.31	2.88
OP	HNϵ (K112)	2.51	2.88	2.72	2.91
OP	HO (Y113)	3.29	2.56	2.94	2.70
OP	HN (L30)	NA	NA	2.99	3.19
base to P distance		5.28	5.19	4.27	4.24
NH_2 to P distance		8.20	7.40	7.94	7.27

[a] Distances in angstroms for computer model of human FBPase−**16** complex; NA = not applicable. [b] Distances in angstroms for X-ray structure of human FBPase−**16** complex (2.0 Å resolution); NA = not applicable. [c] Distances in angstroms for computer model of human FBPase−AMP complex, which was generated using human FBPase−ZMP structure; NA = not applicable. [d] Distances in angstroms for X-ray structure of human FBPase−AMP complex complex (2.3 Å resolution, ref 21a); NA = not applicable.

to the imidazole nitrogen (Table 5). The larger distance between T31 and the imidazole nitrogen of **16** (4.88 Å) appears related to the tilting of the benzimidazole base relative to the adenine of AMP, which presumably is necessary to accommodate the furanyl spacer and the inherently longer C8 to P distance. The furanyl spacer of **16** is engaged in a weak electrostatic interaction with the amide nitrogen of L30, which may at least partially compensate for the loss of the hydrogen bond to the imidazole nitrogen. As shown in Figure 6, the ribose of AMP and the alkyl sidechains of **16** reside in different regions within the AMP binding site and form favorable interactions with different binding site residues. Specifically, the ribose is positioned near the protein−solvent interface with O3′ in some instances forming a hydrogen bond with the guanidine of R140. In contrast, the alkyl substituents of **16** reside near a hydrophobic surface within the AMP binding site and form van der Waals contacts with the sidechains of M177 (S with 7-ethyl, 3.6 Å), L30 (Cδ1 with 1-*i*-butyl, 4.0 Å), and V160 (Cγ1 with 1-*i*-butyl, 3.4 Å).

Inhibition Kinetics. Compounds in Table 2 inhibited FBPase in a concentration-dependent manner. The inhibition kinetic profiles of **16** and AMP were similar with both exhibiting the same maximal FBPase inhibition (∼99%) achieved largely over a narrow concentration range (∼1 log).[18] Moreover, like AMP, **16** exhibited noncompetitive inhibition kinetics (data not shown).

FBPase Specificity. The AMP binding site specificity of **16** was assessed by evaluating the effect of **16** on five AMP-binding enzymes, namely human erythrocytic AMP deaminase, rabbit muscle glycogen phosphorylase, human AMP-activated protein kinase, rabbit muscle adenylate kinase, and rabbit liver phosphofructokinase. No effects were observed at concentrations 1000-fold above the human liver FBPase IC_{50} for **16**. In addition, no significant effects were observed in a screen against >70 enzymes, ion channels, and receptors (Panlabs, Bothel, WA) at 10 μM **16**.

Inhibition of Glucose Production. Freshly isolated rat hepatocytes were used to assess the ability of **16** to penetrate

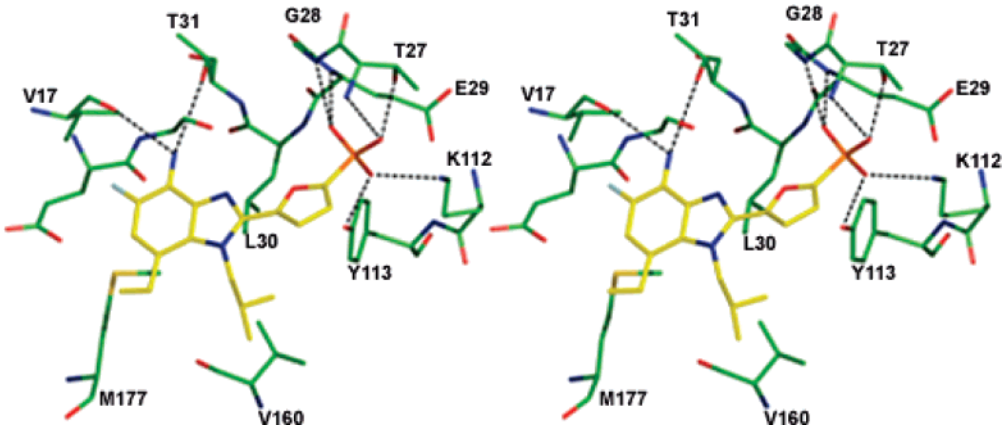

Figure 5. Stereodiagram derived from the X-ray structure of the human FBPase−**16** complex showing the interactions between the AMP binding site of FBPase and **16**. Putative hydrogen bonds are shown as dotted lines when the distance between the acceptor and donor is less than 3.3 Å.

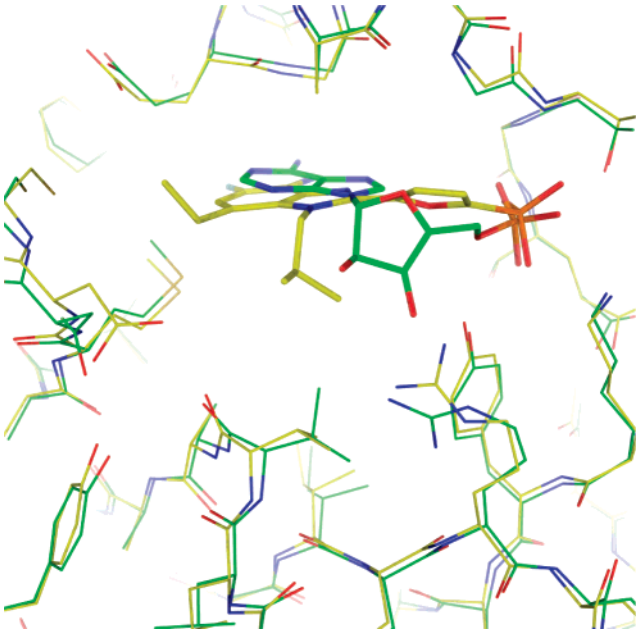

Figure 6. Superimposition of the Cα traces of FBPase from the human FBPase−**16** (carbons colored yellow) and human FBPase−AMP (carbons colored green) complexes. The average rms deviation was 0.55 Å for Cα and 1.02 Å for the sidechains.

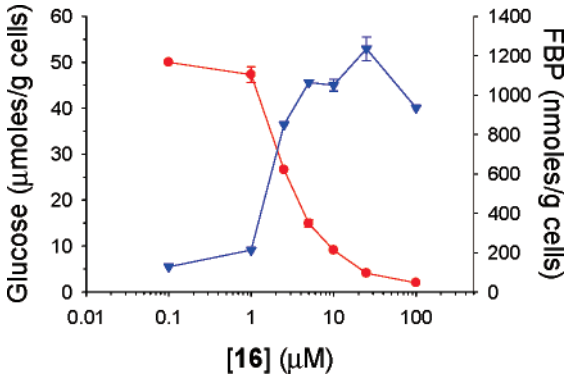

Figure 7. Glucose production from 10 mM lactate/1 mM pyruvate (red ●, IC_{50} = 0.38 ± 0.02 μM) and intracellular fructose-1,6-bisphosphate (FBP) levels (blue ▼) in freshly isolated rat hepatocytes incubated for 1 h with the indicated concentration of **16**.

hepatocytes and inhibit glucose production by an FBPase-dependent mechanism. **16** inhibited glucose production from lactate/pyruvate (gluconeogenesis) in a concentration-dependent manner with an IC_{50} of 2.8 ± 0.5 μM (n = 2 studies, duplicate samples) and a maximal inhibition of approximately 100% relative to vehicle-treated hepatocytes (Figure 7). Inhibition was associated with an approximate 10-fold increase in intracellular fructose-1,6-bisphosphate levels.

Discussion

Our discovery of a series of non-nucleoside AMP mimics with high inhibitory potencies and specificities for FBPase benefited from structural information obtained by X-ray crystallography and molecular modeling studies. Central to our success was the initial recognition that the phosphate binding site was accessible from the purine base using 3-atom spacers to link C8 to the PO_3^{2-}. The inhibitory potency of the initial lead inhibitor, **4** (IC_{50} = 118 μM), was subsequently improved more than 1000-fold through structural modifications in the spacer, ribose, and purine base. Efforts to reduce the desolvation costs and entropic penalty associated with the spacer while gaining affinity through favorable electrostatic interactions led to the discovery of the 2,5-furanyl spacer. The ribose moiety, which became expendable with the spacer strategy, was replaced with less polar alkyl groups capable of forming favorable van der Waals contacts with a hydrophobic surface within the AMP binding site. Last, the purine base was replaced with a substituted benzimidazole. Ultimately, a combination of these structural changes led to the benzimidazole phosphonic acid **16**, an AMP mimic that inhibits FBPase 11-fold more potently than AMP.

Evidence that **16** not only bound to the AMP site of FBPase but also functioned as an AMP mimic was apparent from both X-ray structural data as well as inhibition kinetics. The structural data demonstrated that like AMP, **16** was complexed to the T-state of FBPase. Consistent with the X-ray data, **16** inhibited FBPase in solution to the same extent as AMP (99%) and like AMP was associated with a steep concentration-dependent inhibition curve that exhibited near-complete inhibition of FBPase at concentrations only 10-fold higher than the IC_{10} concentration.

The high FBPase specificity achieved by **16** presumably arose from the large structural differences between **16** and AMP combined with the structural differences between the FBPase AMP binding site and the binding sites for other AMP-binding enzymes. A review of X-ray structures of nucleotide binding

sites[32] and more specifically of AMP binding sites suggested that the origin of this high specificity may arise from the combined effects of several structural changes. Linking C8 of the adenine base to PO_3^{2-} by a 3-atom spacer may be the largest single contributor to the increased specificity, since its success depended on the preference of FBPase to bind AMP in the *anti*, +*sc*, -*ac* conformation[31] and correspondingly on the angle and distance between C8 and the phosphorus atom. AMP binding sites favoring different AMP binding conformations correspondingly favor different distances and/or angles[33b] between the base and PO_3^{2-} and therefore are unlikely to recognize compounds that link the base and PO_3^{2-} by the rigid 2,5-furanyl spacer. Specificity is also attributed to differences in AMP binding site interactions with the purine and ribose moieties. Unlike many other nucleotide binding sites, FBPase binds AMP by forming hydrogen bonds with N7 and the $^6NH_2$ group but not N1 or N3. In addition, the replacement of the ribose with an alkyl or an alkylaryl group eliminates binding to AMP binding sites that require interactions with the ribose for high affinity or are unable to accommodate hydrophobic groups near N9.

The final step prior to designating **16** as the lead AMP mimic was demonstration of cellular uptake and inhibition of intracellular FBPase activity. Phosphonic acids usually fail to enter cells due to their high negative charge at physiological pH. Fortunately, the cells that produce glucose via the gluconeogenesis pathway, i.e., liver and kidney cells, contain cell surface transporters known as organic anion transporters that often aid the uptake and elimination of negatively charged compounds.[33] Results from studies with primary rat hepatocytes demonstrated that **16** is rapidly transported into hepatocytes. Cell penetration was subsequently confirmed by studies showing that **16** inhibited the conversion of lactate/pyruvate to glucose in a concentration dependent manner and that this inhibition was via FBPase based on the corresponding rise in intracellular levels of fructose-1,6-bisphosphate.

The discovery of **16** highlights the value of structure-based drug design, especially in light of the apparent difficulty in finding suitable AMP mimics by screening large compound libraries. The X-ray structure of the human FBPase−AMP complex provided the initial understanding of the AMP binding site interactions, whereas FEP calculations[24] added important insights into the contribution of each individual interaction to the overall binding affinity. Molecular modeling helped guide medicinal chemistry efforts to retain the key binding site interactions formed by AMP while attempting to exploit other features within the binding site that could enhance either binding site affinity or specificity. The early decision to focus on phosphonic acids stemmed from the recognition that the phosphate binding site interactions were very important to the overall binding affinity and that the phosphate binding site was most compatible with a negatively charged tetrahedral group. Discovery of the initial lead, **4**, was guided by modeling studies demonstrating that the phosphate binding site was accessible from the C8 carbon on the adenine base. Subsequent modeling studies provided additional information that aided in the spacer optimization and the selection of 3-atom spacers that could bridge the space between the purine base and PO_3^{2-} group in a manner that simultaneously preserved the favorable interactions between these groups and their respective biding sites. Modeling studies and FEP calculations also provided the incentive to replace the purine base with a benzimidazole and the ribose with alkyl groups to minimize desolvation costs and gain van der Waals interactions. Importantly, the binding site interactions predicted by computer modeling and used as an integral part of our design process nearly 10 years ago were replicated experimentally when the structure of the FBPase−**16** complex was solved recently by X-ray crystallography.

As described in the subsequent article,[17] this work was followed by a substantial lead optimization effort that led to the discovery of MB05032 and an orally bioavailable phosphonic diamide prodrug of MB05032, MB06322 (designated as CS-917). CS-917 was shown to lower glucose in animal models of mild and severe diabetes.[18,19] Moreover, CS-917 resulted in pronounced glucose lowering in type 2 diabetics[20] and may therefore represent an important new therapy for this growing and costly disease that afflicts nearly 170 million people worldwide.

Conclusions

AMP binding sites represent potential drug targets that remain largely unexplored due to long-standing difficulties in finding potent, selective, and cell penetrable compounds. FBPase is one such AMP-binding enzyme that has received considerable attention based on its potential as a drug target for type 2 diabetes, but without success. To address this drug discovery challenge, we used several X-ray structures of FBPase-inhibitor complexes and numerous computer modeling studies to guide the design of a series of AMP mimics that bear little structural resemblance to AMP. The lead compound, **16**, was shown to inhibit FBPase 11-fold more potently than AMP and to exhibit high specificity for FBPase. Moreover, **16** was shown to undergo rapid uptake by rat hepatocytes, which resulted in potent inhibition of FBPase and glucose production via the gluconeogenesis pathway. These results suggest that AMP mimics with suitable drug-like properties are achievable and therefore that AMP-binding sites represent potential drug targets worthy of further exploration.

Experimental Procedures

General Methods. All moisture-sensitive reactions were performed under a nitrogen atmosphere using oven-dried glassware and anhydrous solvents purchased and used without further manipulation. TLC was performed on Merck silica gel 60 F_{254} TLC glass plates and visualized with UV light or a suitable stain. Flash chromatography was performed on 230−400 mesh EM Science silica gel 60. Melting points were recorded on a Thomas-Hoover capillary melting point apparatus and are uncorrected. ^1H, ^{13}C, and ^{31}P NMR spectra were recorded on Varian Gemini or Mercury spectrometers operating respectively at 200 or 300 MHz for proton, 50 or 75 MHz for carbon, and 121 MHz for phosphorus spectra. Analytical HPLC was performed on a 4.6 × 250 mm YMC ODS-AQ 5 μm column eluting with a 0.1% aqueous AcOH/MeOH gradient at a flow rate of 1 mL/min and the detector set at 280 nm. Mass spectrometry data were determined at Mass Consortium Corp. (San Diego, CA) or on a Perkin-Elmer Sciex API2000 LC-MS system. Elemental microanalyses were performed by NuMega Resonance Labs, Inc. (San Diego, CA) or by Robertson Microlit Laboratories (Madison, NJ).

[5-(7-Bromo-5-fluoro-1-isobutyl-4-nitro-1*H*-benzimidazol-2-yl)-furan-2-yl]-phosphonic Acid Diethyl Ester (19). A solution of

(32) (a) Moodie, S. L.; Mitchell, J. B.; Thornton, J. M. *J. Mol. Biol.* **1996**, *263*, 486−500. (b) Moodie, S. L.; Thornton, J. M. *Nucleic Acids Res.* **1993**, *21*, 1369−1380.

(33) van Montfoort, J. E.; Hagenbuch, B.; Groothuis, G. M.; Koepsell, H.; Meier, P. J.; Meijer, D. K. *Curr. Drug Metabol.* **2003**, *4*, 185−211.

6-bromo-4-fluoro-3-nitrobenzene-1,2-diamine (**18**, 94.0 g, 375 mmol) in 1,2-dichloroethane (950 mL) at 0 °C was treated with isobutyraldehyde (27.1 g, 375 mmol) followed by sodium triacetoxyborohydride (159 g, 750 mmol) and then dropwise with glacial acetic acid (84.0 mL, 1460 mmol) over 15 min while maintaining the temperature between 0 and 5 °C.[34] After stirring at 0 °C for an additional hour, the resulting mixture was quenched with a saturated $NaHCO_3$ solution and extracted with EtOAc (3 × 750 mL). The combined organic extracts were washed with water (2 × 1 L) and brine (750 mL), dried ($MgSO_4$), filtered, and concentrated under reduced pressure. The resulting residue was coevaporated with toluene (750 mL) to afford a brown oil (113 g, 98%). ^{1}H NMR (DMSO-d_6): δ 0.93 (d, 6H, J = 6.6 Hz), 1.8 (m, 1H), 2.53 (m, 2H), 3.87 (br s, 1H, D_2O exchangeable), 6.78 (br s, 2H, D_2O exchangeable), 6.88 (d, 1H, J = 11.6 Hz). The above material (90.8 g, 296 mmol) was dissolved in DMF (500 mL) and treated with 5-diethylphosphono-2-furaldehyde (75.6 g, 325 mmol). Air was bubbled through the solution while iron (III) chloride (52.8 g, 325 mmol) was added portionwise.[35] Air bubbling was continued while the resulting dark mixture was stirred and heated at 90 °C. After 2 h, the mixture was cooled to room temperature and the solvent was evaporated under reduced pressure. The dark oil was coevaporated with toluene (3 × 200 mL), and the residue was dissolved in EtOAc (3.0 L). The EtOAc solution was washed with water (3 × 600 mL) and brine (600 mL) and then dried ($MgSO_4$), filtered, and concentrated under reduced pressure to provide a dark tar. The crude material was purified by chromatography on silica gel (2.0 kg, 6 in. diameter column) using 40−60% EtOAc: hexanes as eluting solvents to give **19** as a brown solid (80.0 g, 52%). ^{1}H NMR (DMSO-d_6): δ 0.8 (d, 6H, J = 6.6 Hz), 1.26 (t, 3H, J = 7.0 Hz), 2.1 (m, 1H), 4.12 (m, 4H), 4.72 (d, 2H, J = 7.8 Hz), 7.48 (m, 2H), 7.93 (d, 1H, J = 11.0 Hz).

[5-(5-Fluoro-1-isobutyl-4-nitro-7-vinyl-1*H*-benzimidazol-2-yl)furan-2-yl]-phosphonic Acid Diethyl Ester (20). A solution of **19** (80.0 g, 154 mmol) in DMF (650 mL) was treated with dichloro bis-(triphenylphosphine)palladium(II) (4.5 g, 6.4 mmol). Nitrogen was bubbled through the stirred mixture while tributylvinyl tin (51.5 mL, 176 mmol) was slowly added. After the addition was complete (5 min), the mixture was warmed to 70 °C and stirred for 1 h with continued nitrogen purge. The mixture was cooled to room temperature and concentrated under reduced pressure. The resulting dark oil was dissolved in EtOAc (2.1 L) and treated with a mixture of sodium fluoride (113 g, 2690 mmol) in water (475 mL). After stirring for 16 h, the mixture was diluted with water (350 mL) and filtered through a pad of Celite in a Buchner funnel (11 cm). The layers were separated, and the aqueous phase was extracted with EtOAc (800 mL). The combined organic extracts was washed with water (600 mL) and brine (600 mL), dried ($MgSO_4$, 125 g), filtered, and concentrated under reduced pressure to give a dark oil (88.6 g). The crude material was purified by chromatography on silica gel (1.75 kg, 6 in. diameter column) using 3:1 EtOAc−hexanes (16 L) as the eluting solvents to give **20** as a pale-orange powder (66.7 g, 92%). mp 77−78.5 °C. ^{1}H NMR (DMSO-d_6): δ 0.73 (d, 6H, J = 6.6 Hz), 1.25 (t, 3H, J = 7.0 Hz), 1.9 (m, 1H), 4.1 (m, 4H), 4.58 (d, 2H, J = 7.8 Hz), 5.7 (d, 1H, J = 9.4 Hz), 6.0 (d, 1H, J = 11.5 Hz), 7.3−7.6 (series of m, 4H).

[5-(4-Amino-7-ethyl-5-fluoro-1-isobutyl-1*H*-benzoimidazol-2-yl)-furan-2-yl]-phosphonic Acid (16). A solution of **20** (57.1 g, 122 mmol) in ethanol (425 mL) was treated with palladium on carbon (4.5 g) under a continuous flow of nitrogen. The resulting mixture was then stirred under one atmosphere of hydrogen for 20 h at room temperature. The reaction mixture was flushed with nitrogen and filtered through a pad of Celite, and the filtrate was concentrated under reduced pressure to provide a thick, orange syrup. The material was dissolved in toluene (250 mL) and filtered through a pad of Celite. The filtrate was concentrated under reduced pressure to give an orange syrup (56 g, 100%), which was used in the next step without further purification. ^{1}H NMR (DMSO-d_6): δ 0.73 (d, 6H, J = 6.6 Hz), 1.05−1.35 (m, 6H), 1.85 (m, 1H), 2.82 (q, 2H, J = 7.0 Hz), 4.1 (m, 4H), 4.38 (d, 2H, J = 7.8 Hz), 5.18 (br s, 2H, exchangeable with D_2O), 6.8 (d, 1H, J = 11.5 Hz), 7.2 (m, 1H), 7.4 (m, 1H).

A solution of the above material in dichloromethane (500 mL) was cooled to 0 °C and slowly treated with bromotrimethylsilane (112 mL, 848 mmol). After warming to room temperature and stirring for 16 h, the solvent was evaporated under reduced pressure to afford a residue that was subsequently coevaporated with acetone (200 mL). Water (800 mL) and acetone (150 mL) were added to the resulting thick, orange tar, and the suspension was stirred vigorously. After 2 h, the suspension was filtered, and the solid was collected, washed with water (3 × 150 mL), and dried under vacuum to give crude **16** as a fine, yellow powder (48.1 g, 103%). ^{1}H NMR (DMSO-d_6): δ 0.69 (d, 6H, J = 6.6 Hz), 1.21 (t, 3H, J = 7.2 Hz), 1.8 (m, 1H), 2.82 (q, 2H, J = 7.2 Hz), 4.38 (d, 2H, J = 7.8 Hz), 6.83 (d, 1H, J = 12.8 Hz), 7.0 (m, 1H), 7.1 (m, 1H).

Crude **16** (114.7 g, obtained by combining several batches) was treated with aqueous sodium hydroxide (1 M, 570 mL, 570 mmol). After stirring at room temperature for 2 h, the cloudy, dark-orange solution was extracted with EtOAc (2 × 350 mL). The dark-orange aqueous phase was then diluted with methanol (350 mL) and treated with activated carbon (Norit SA-3, 4.0 g). The mixture was filtered twice through Celite and once through filter paper. The filtrate (1.4 L total volume) was treated with concentrated hydrochloric acid (48 mL, 570 mmol) dropwise with vigorous stirring. A persistent yellow precipitate formed during the second half of the addition. After the addition was complete (45 min), the mixture was stirred at room temperature for 2 h and then at 0 °C for 1 h. The solid was collected by filtration and washed with MeOH−water (60:40, 100 mL) and then water (3 × 200 mL). The solid was dried under vacuum to give **16** as a fine, yellow-orange powder (93.4 g, 86%). mp >220 °C. ^{1}H NMR (DMSO-d_6): δ 0.68 (d, 6H, J = 6.6 Hz), 1.21 (t, 3H, J = 7.2 Hz), 1.7−2.0 (m, 1H), 2.83 (q, 2H, J = 7.2 Hz), 4.37 (d, 2H, J = 7.4 Hz), 6.83 (d, 1H, J = 12.8 Hz), 7.02 (m, 1H), 7.12 (m, 1H). ^{13}C NMR (DMSO-d_6): δ 15.79, 19.25, 23.59, 30.47, 52.08, 112.66, 112.89, 113.1, 114.86, 115.00, 119.64, 120.10, 124.43, 124.73, 129.77, 133.49, 133.67, 143.15, 143.32, 147.65, 147.81, 148.02, 149.16, 153.66. $[MH]^+$ calcd for $C_{17}H_{21}N_3O_4PF$: 382. Found: 382. Anal. calcd for $C_{17}H_{21}N_3O_4PF$: C, 53.54; H, 5.55; N, 11.02; F, 4.98. Found: C, 53.27; H, 5.47; N, 10.92; F, 4.92.

Computational Details. All molecular dynamics, molecular mechanics, and free-energy perturbation calculations were carried out with the AMBER program using an all atom force field[36] and the SPC/E model potential[37] to describe water interactions. Procedures for generating the computer model of the FBPase complexes and for developing all force field parameters for nonstandard residues are as described previously and detailed in the Supporting Information.

Spacer groups were evaluated computationally starting with the three-dimensional structure of the human FBPase−ZMP complex[22a] and later complexes of FBPase with **4** and **11**. The ZMP complex was used to generate a computer model of the FBPase−AMP complex.[24] AMP was replaced with analogs denoted in Table 1 by positioning the phosphonate in the phosphate binding site in a manner that retained the full complement of hydrogen bonds. Low-energy spacer conformations were selected that positioned the adenine base and the ribose in the general vicinity of where they bound in the AMP complex. The complex was

(34) The order of reagent addition and addition times are critical for successful conversion. The addition of acetic acid before the reducing agent results in exclusive formation of the dihydrobenzimidazole.

(35) An exotherm was observed during the iron (III) chloride addition.

(36) (a) Weiner, S. J.; Kollman, P. A.; Case, D. A.; Singh, U. C.; Ghio, C.; Alagoha, G.; Profeta, S., Jr.; Weiner, P. K. *J. Am. Chem. Soc.* **1984**, *106*, 765−784. (b) Singh, U. C.; Weiner, P. K.; Caldwell, J. K.; Kollman, P. A. *AMBER Version 3.0*; University of California at San Francisco: San Francisco, CA, 1986.

(37) (a) Berendsen, H. J. C.; Grigera, J. R.; Straatsma, T. P. *J. Phys. Chem.* **1987**, *91*, 6269−6271. (b) Reddy, M. R.; Berkowitz, M. *J. Chem. Phys.* **1988**, *88*, 7104−7110.

then energy minimized using a four-stage protocol and the BORN module of the AMBER program. Energy minimization at each stage entailed 500 steps of steepest descent followed by 2000 steps of conjugate gradient. In stage one, the inhibitor and protein were fixed and only the water molecules were minimized to relieve any bad contacts that arose as a result of solvating the system. In stage two, all heavy atoms were fixed and only the hydrogens were allowed to relax to obtain optimal hydrogen bond geometries and interactions. In stage three, atoms associated with the protein and atoms that coincide with AMP atoms were fixed whereas the remaining atoms and water molecules were left unrestrained. Last, in stage four, all residues within 25 Å from the center of the AMP mimic were allowed to relax.

A four-stage protocol was also used in the energy minimization of the solvated inhibitor. Energy minimization was carried out using periodic boundary conditions in all directions. Each stage entailed 500 steps of steepest descent and 2000 steps of conjugate gradient. Similar to above, stage one minimized the water molecules while keeping the inhibitor fixed, stage two relaxed the hydrogen atoms, stage three fixed only the ligand atoms in common with the molecule (AMP, **4** or **11**) in the X-ray structure, and stage four allowed all atoms to relax.

The minimized structures for all the inhibitors in the complex and solvated states were used for calculating the following energy differences:

$$\Delta E_{\text{bind}}\,(\text{intra}) = E_{\text{com}}(\text{intra}) - E_{\text{sol}}(\text{intra}) \quad (1)$$

$$\Delta E_{\text{bind}}\,(\text{inter}) = E_{\text{com}}(\text{inter}) - E_{\text{sol}}\,(\text{inter}) \quad (2)$$

$$\Delta E_{\text{bind}}\,(\text{total}) = \Delta E_{\text{bind}}\,(\text{intra}) + \Delta E_{\text{bind}}\,(\text{inter}) \quad (3)$$

where, ΔE_{bind}(intra) and ΔE_{bind}(inter) are relative intra- and intermolecular binding interaction energies of an inhibitor, respectively, and where E_{com}(intra), E_{com}(inter), E_{sol}(intra), and E_{sol}(inter) are intra- and intermolecular interaction energies of an inhibitor in the complex and solvated states, respectively. ΔE_{bind} (total) is the total binding energy of an inhibitor.

Free-energy calculations were conducted as previously described.[24,38] Prior to the mutation, the system was minimized using the four-stage protocol followed by an equilibration period using 20 ps of MD simulation and a 2 fs time step. Mutations suitable for the single topology method were conducted using 51 windows with each window comprising 3 ps of equilibration and 6 ps of data collection or a total of 479 ps of MD simulation. The double topology method[30] was used for mutations involving larger structural changes. In this case, calculations entailed two stages with each stage using 51 windows and each window comprising 2 ps of equilibration and 4 ps of data collection or a total of 632 ps of MD simulation. Each mutation followed the doublewide sampling procedure, and the results reported are based on the averages from the backward and forward simulations of the mutation. Errors were estimated for each window by dividing the window statistics into four groups (in both forward and backward directions) and computing the standard deviation for the indicated free-energy change. The root-mean-square of these window errors are reported as a measure of the statistical uncertainty in the result for each mutation.

Biological Assays. FBPase activity and the activity of the AMP-binding enzymes human erythrocytic AMP deaminase, rabbit muscle glycogen phosphorylase, human AMP-activated protein kinase, rabbit muscle adenylate kinase, and rabbit liver phosphofructose kinase were measured as previously described[18] and as detailed in the Supporting Information. FBPase IC_{50} values were calculated by 4-parameter logistics regression analysis of plots of FBPase activity versus inhibitor concentration using Statview software (SAS Institute, Cary, NC).

Glucose production from freshly isolated rat hepatocytes was measured as previously described[18] after a 1 h incubation with **16**. Intracellular fructose-1,6-bisphosphate levels were determined enzymatically at the same timepoint using aldolase- and triosephosphate isomerase-containing reactions that coupled the production of glyceraldehyde 3-phosphate to the oxidation of NADPH.

Source of FBPase and Crystal Growth. The pET3a expression vector containing the human liver FBPase gene was a gift from M. Raafat El-Maghrabi (State University of New York, Stony Brook). The enzyme was expressed in *Escherichia coli* containing this vector and purified to homogeneity as previously described.[21a] Crystals of the FBPase−**16** complex were grown at room temperature by the hanging drop method: 2 μL FBPase (24 mg/mL) in buffer (2.7 mM **16**, 5 mM sodium malonate, pH 7.2, 1 mM dithiothreitol, 0.5 mM phenylmethylsulfonyl fluoride, 0.1 mM EDTA, and 2 mM fructose-1,6-bisphosphate) was mixed with 2 μL of 6% (vol/vol) polyethylene glycol 8000 (PEG-8K)/0.1 M Tris-HCl (pH 8.2), and equilibrated against 1 mL 6% PEG-8K/0.1 M Tris-HCl (pH 8.2). The following day, the resulting crystals were soaked in 20% glycerol/80% crystallographic buffer (6% PEG-8K/0.1 M Tris-HCl, pH 8.2) (vol/vol) for about 5 s, plunged into liquid nitrogen (77 K), and then stored until data collection.

Data Collection and Analysis. The diffraction data were collected at 100 K on beamline F-1 of the Cornell High-energy Synchrotron Source (CHESS). The crystal was in the space group $P2_1$. There are two tetramers in the asymmetric unit. A search model was obtained from the PDB code 1FTA.[21a] Molecular replacement was then carried out by using AMORE.[39] The model of **16** was generated by CS Chem3D Pro (http://www.camsoft.com), modified according to the electron density in the simulated annealing omit map, and the conformation of the model was optimized by energy minimization in CS Chem3D Pro. The structure of human liver FBPase complexed with **16** was refined by using the CNS_SOLVE package.[40] The model was then visualized and refined against 2Fo-Fc and Fo-Fc maps by using the program O.[41] The stereochemical properties of the intermediate and the final structures were examined by PROCHECK.[42] In the final structure, 89.8% residues were in the most favored regions, 9.9% residues were in additional allowed regions, and 0.3% residues were in generously allowed regions.

Acknowledgment. We thank Dr. Edward Robinson, Dr. Gerard Scarlato, Brian Brown, Dr. Raja Reddy, Yan Liu, Wei Xiao, Jay DaRe, Joe Kopcho, and Robert Rydzewski for their assistance in compound synthesis; Tim Colby and Emily Topczewski for characterization of the compounds in the biological assays; and Dr. Sridhar Prasad for graphical representations of the binding interactions.

Supporting Information Available: Analytical data and procedures for the preparation of compounds **3**−**15** and intermediates generated during the synthesis of **16**. Enzyme assays and rat hepatocyte assays. Procedure for developing force field parameters for nonstandard residues, as well as procedures for energy minimizations in solvent and the complex and for the development of the computer models of FBPase complexed with AMP and **16**. Complete ref 8b. This material is available free of charge via the Internet at http://pubs.acs.org.

JA074869U

(38) Reddy, M. R.; Erion, M. D.; Agarwal, A. In *Reviews in Computational Chemistry*; Lipkowitz, K. B., Boyd, D. B., Eds.; Wiley-VCH: New York, 2000; Vol. 16, pp 217−304.

(39) Navaza, J. *Acta Cryst.* **1994**, *A50*, 157−163.

(40) Brunger, A. T.; Adams, P. D.; Clore, G. M.; DeLano, W. L.; Gros, P.; Grosse-Kunstleve, R. W.; Jiang, J.-S.; Kuszewski, J.; Nilges, N.; Pannu, N. S.; Read, R. J.; Rice, L. M.; Simonson, T.; Warren, G. L. *Acta Cryst.* **1998**, *D54*, 905−921.

(41) Jones, T. A.; Zou, J.-Y.; Cowan, S. W.; Kjeldgaard, M. *Acta Cryst.* **1991**, *A47*, 110−119.

(42) Laskowski, R. A.; MacArthur, M. W.; Moss, D. S.; Thornton, J. M. *J. App. Cryst.* **1993**, 26, 283−291.